Supporting Information

Reaction of O_2 with a di-iron protein generates a mixed valent Fe^{2+}/Fe^{3+} center and peroxide

Justin M. Bradley, Dimitri A. Svistunenko, Jacob Pullin, Natalie Hill, Rhona K. Stuart, Brian Palenik, Michael T. Wilson, Andrew M. Hemmings, Geoffrey R. Moore and Nick E. Le Brun

www.pnas.org/cgi/doi/10.1073/pnas.1809913116

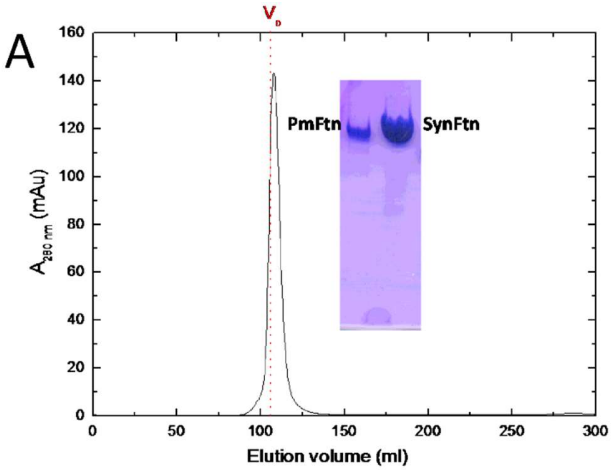

B

```
                  *         20        *         40        *         60        *         80        *
SynFtn     : MATDVAQGPNGRALAESMNPDLLSAHQQHLSHFRYASVTYTAMSYYCAE--RELAGFYQFFDGEAKDPQSFAVHFTQYLIARSQSNDLQT :  88
HumanH     : ~~~~~MTTASTSQVRQNYHQDSEAAINRQINLELYASYVYLSMSYYFDRDDVALKNFAKYFLHQSHEERESAEKLMKLQNQRGGRIFLQD :  85
MouseH     : ~~~~~MTTASPSQVRQNYHQDAEAAINRQINLELYASYLYLSMSCYFDRDDVALKNFAKYFLHQSHGERESAEKIMKLQNQRGCRIFLQD :  85
FrogM      : ~~~~~~~~~MVSQVRQNYHSDCEAAVNRMLNLELYASYTYSSMYAFFDRDDVALHNVAEFFKEHSHEERESAEKFMKYQNKRGGRVVLQD :  81
Ecoli      : ~~~~~~~~~~~~~~~~~MLKPEMIEKLNEQVNLELYSSLTYQQMSAWCSY--HTFEGAAAFLRRHAQEEMTEMQRIFDYLTDTGNLPRINT :  72
Cjejuni    : ~~~~~~~~~~~~~~~~~MLSKEVVKLLNEQINKEMYAANTYTSMSSWCYE--NSLDGAGAFLFAHASEESDEANKLITYLNETDSHVELQE :  72
Hpylori    : ~~~~~~~~~~~~~~~~~MLSKDIIKLLNEQVNKEMNSSNTYYSMSSWCYT--HSLDGTGLFLFDHAAEEYEHAKKLIVFLNENNVPVQLTS :  72
Vcholerae  : ~~~~~~~~~~MNQEFFMLSQAMVEHLNEQINLEFTSSNLYLQMSAWCED--KGFDGAAEFLRAHAVEEMQHMQRLFTYVSETGALPILGA :  78
Ypestis    : ~~~~~~~~~~~~~~~~~MLKKEMAQKLNEQLNLEFYSANLYLQMSAWCSD--KGFEGAAAFLKKHSQEEMQHMERLFEYLSGTGSMPVLGT :  72

                 100        *        120        *        140        *        160        *        180
SynFtn     : IDAER-QNWDSLASLMATAFQMEADITSSIQSVYALAERNSFIRTTVFIDD-PLIEAQIQSEDQFAYLLGRYKFANG--DPTALLVIDNEL : 174
HumanH     : IKKEDCDDWESGLNAMECALHLEKNVNQSLLELHKLATDKNDPHLCDFIETHYLNEQVKAIKELGDHVTNLRKMGAPESGLAEYLFDKHT : 175
MouseH     : IKKEDRDDWESGLNAMECALHLEKSVNQSLLELHKLATDKNDPHLCDFIETYYLSEQVKSIKELGDHVTNLRKMGAPEAGMAEYLFDKHT : 175
FrogM      : IKKEERDEWGNTLEAMQAALQLEKTVNQALLDLHKLATDKVDPHLCDFLESEYLEEQVKDIKRIGDFITNLRKLGLPENGMGEYLFDKHS : 171
Ecoli      : VESEF-AEYSSLDELFQETYKHEQLITQKLNELAHAAMTNQDYPTFNFLQ-WYVSEQHEEEKLFKSILDKLELAGK--SGEGLYFIDKEL : 158
Cjejuni    : VKQEE-QNFKSLLDVFEKTYEHEQFITKSTNTLVEHMLTHKDYSTFNFLQ-WYVSEQHEEEALFRGTVDKIKLTGE--HGNGLYLADQYT : 158
Hpylori    : ISAEE-HKEEGLTQIFQKAYEHEQHISESTNNIVDHAIKSKDHATFNFLQ-WYVAEQHEEEVLFKDILDKIELIGN--ENHGLYLADQYV : 158
Vcholerae  : IAAER-HEEASLGEVFRETYLHEQKITQQLNKLAHVAFTSQDYSTFNFLQ-WYVAEQHEEEKLFKGILDKLELVGE--DGKALFFIDKDL : 164
Ypestis    : ITAEP-VDFASLADVFKLTYEHEQLITTQLNFLAHVAMTTHDYSTFNFLQ-WYVAEQHEEEKLFKSTLDKLALVGN--SGNSLFFVDKDL : 158
```

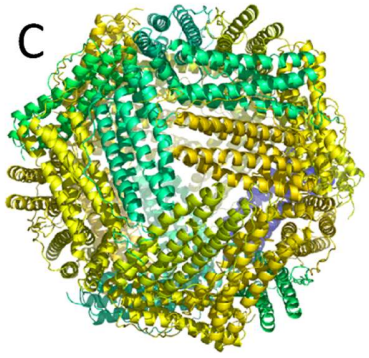

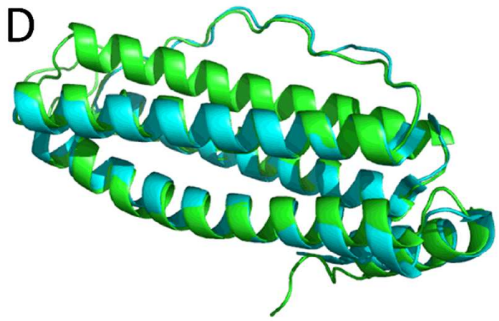

Figure S1. Association state and structure of *Syn*Ftn. (**A**) Elution profile of the purified protein from a HiPrep 26/60 Sephacryl S-200HR size exclusion column. The red dashed line indicates the void volume of the column as determined using blue dextran. Least squares analysis gave a line of best fit describing the ratio of elution to void volume of -0.702 × log(rmm) +4.84 (R^2 = 0.982). *Syn*Ftn eluted in a single peak close to the void volume of the column at 110 mL suggesting a molecular mass of >270 kDa (predicted mass for a 24meric assembly based on monomer sequence is 485 kDa). Thus, under the conditions of the measurements reported here, *Syn*Ftn exists in a single association state most likely corresponding to the fully assembled 24mer. Inset is a comparison between *Syn*Ftn and a sample of Ftn from *Pseudo-nitzschia multiseries* (PmFtn), which is known to form 24meric assemblies with a molecular weight 530 kDa (1) using native PAGE. Again, *Syn*Ftn ran as a single band suggesting only one association state of the protein and this permeated approximately the same distance into the gel as PmFtn. (**B**) Comparison of the sequence of *Syn*Ftn with those of selected prokaryotic and animal ferritins. Red arrows indicate the residues serving as ligands to site C in prokaryotic ferritins, black arrows the ligands to the diiron site present in all H-chain ferritins and the green shaded region highlights the position of the carboxylate rich patch characteristic of L-chain and phytoferritins. The black circle indicates the tyrosine residue that is conserved in all H-chain ferritins (Y40 in *Syn*Ftn). Proteins are human H-chain ferritin (HumanH), mouse H-chain ferritin (mouseH), frog M-chain ferritin (FrogM), *E. coli* FtnA (Ecoli), *Campylobacter jejuni* Ftn (Cjejuni), *Helicobacter pylori* Ftn (Hpylori), *Vibrio cholerae* Ftn (Vcholerae), and *Yesinia pestis* Ftn (Ypestis). (**C**) The biological assembly of 24 monomeric units arranged to form a rhombic dodecahedron, viewed along one of eight 3-fold axes. (**D**) An overlay of the structure of one *Syn*Ftn monomer (green) with a monomer of *E. coli* FtnA (cyan).

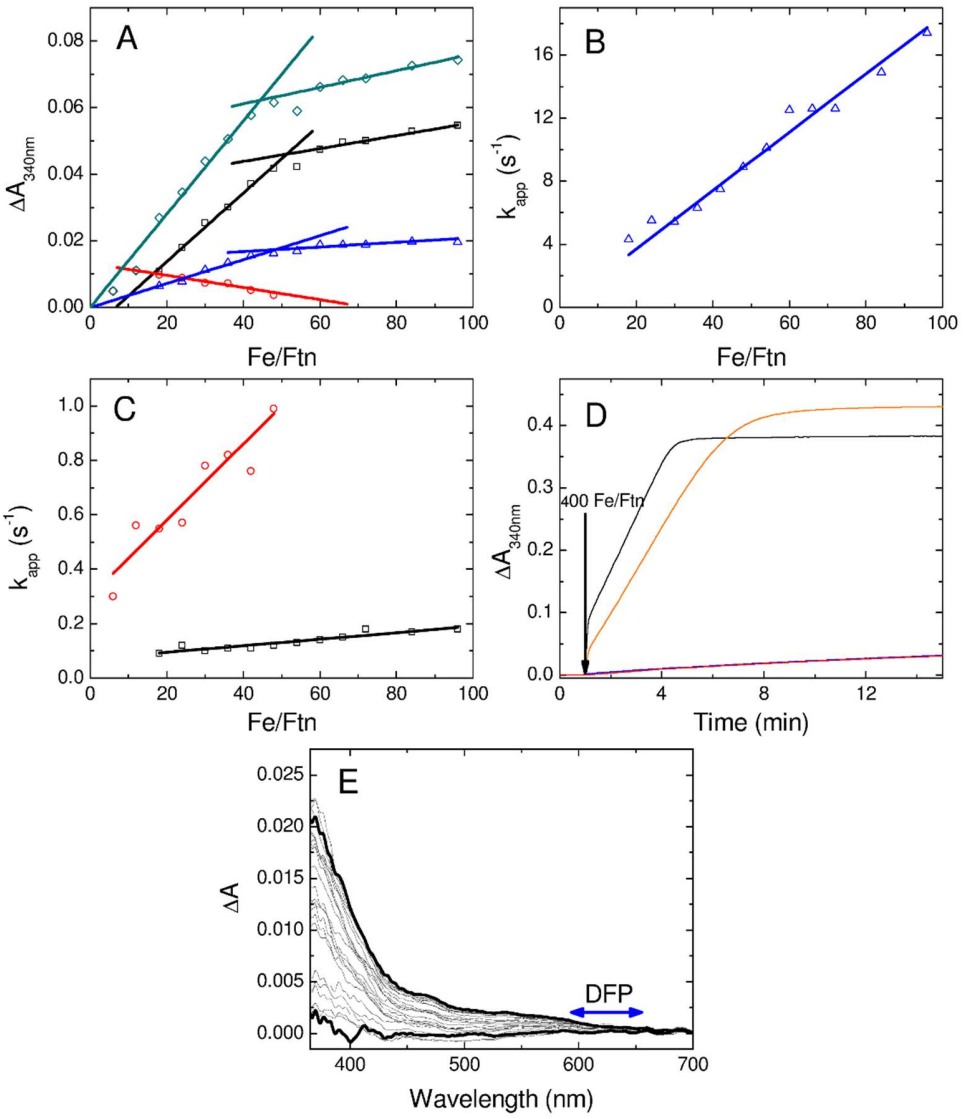
A
ΔA340nm
Fe/Ftn
B
kapp (s-1)
Fe/Ftn
C
kapp (s-1)
Fe/Ftn
D
ΔA340nm
400 Fe/Ftn
Time (min)
E
ΔA
DFP
Wavelength (nm)

Figure S2. Rate analysis of iron oxidation by *Syn*Ftn proteins. At iron loadings of 0.5 Fe^{2+} per ferroxidase center (12 Fe^{2+} per *Syn*Ftn) or lower the UV-visible absorbance data were well described by a single exponential function. The apparent rate constant associated with this process, k_i (0.3 – 1.0 s^{-1}), increased with the ratio of Fe^{2+} to protein. However, at loadings above 0.5 Fe^{2+} per ferroxidase center, the corresponding amplitude of the absorbance change decreased in parallel with the onset of a second process of iron oxidation that could only be satisfactorily described using a bi-exponential function characterized by rate constants k_r and k_s. The iron dependence was such that only the amplitude of the latter increased at loadings above 2.0 Fe^{2+} per ferroxidase center (48 Fe^{2+} per *Syn*Ftn), sufficient to saturate all binding sites. Under these conditions iron oxidation was biphasic, consisting of a rapid phase for which the apparent rate constant, k_r, increased linearly with concentration of Fe^{2+} (4.3 to 17 s^{-1}) and a slow phase the rate constant for which, k_s, was almost independent of Fe^{2+} concentration (0.09 to 0.18 s^{-1}). (**A**) Amplitude of the absorbance change measured by stopped flow at 340 nm associated with the slow (black), intermediate (red) and rapid (blue) phases of iron oxidation together with the total observed amplitude change (dark cyan) as a function of Fe^{2+} added per *Syn*Ftn. Trend lines represent linear fits to the data. The absorbance change associated with rapid oxidation reached a maximum of 0.018 absorbance units and saturated at an iron loading of approximately 2 Fe^{2+} per ferroxidase center. The amplitude of the absorbance change associated with slow oxidation did not saturate at loadings up to 4 Fe^{2+} per ferroxidase center (96 Fe^{2+} per SynFtn) but there was a marked decrease in its iron dependence above 2 Fe^{2+} per ferroxidase center. (**B**) and (**C**) Apparent rate constants extracted for the rapid (**B**), intermediate and slow (**C**) phases of iron oxidation (k_r, k_i and k_s from Equation 1 and as defined above) as a function of Fe^{2+} added per *Syn*Ftn. Protein (1.0 μM in 100 mM MES pH 6.5) was mixed with equal volumes of Fe^{2+} at the appropriate concentration and stabilized in 1 mM aqueous HCl. (**D**) Iron mineralization in *Syn*Ftn variants. Absorbance monitored iron oxidation following the addition of 400 equivalents of Fe^{2+} to 0.5 μM wild type *Syn*Ftn (black trace) and variants Y40F (orange), E33A (blue) and E110A (red), in 100 mM MES pH 6.5. Note that the latter two variants' traces overlay almost completely. (**E**) Formation of a DFP intermediate during iron oxidation by *Syn*Ftn is not detectable by stopped flow absorbance. Spectra (360-700 nm) of 3 μM *Syn*Ftn recorded during the first 80 milliseconds following mixing of apo protein with 48 equivalents of Fe^{2+}. The increase in absorbance over time at low wavelengths reports on iron oxidation via the broad feature due to oxo-coordinated Fe^{3+} species. However, no corresponding discrete absorbance feature is detected in the range expected (600-650 nm, indicated by the blue double headed arrow) for formation of a DFP species.

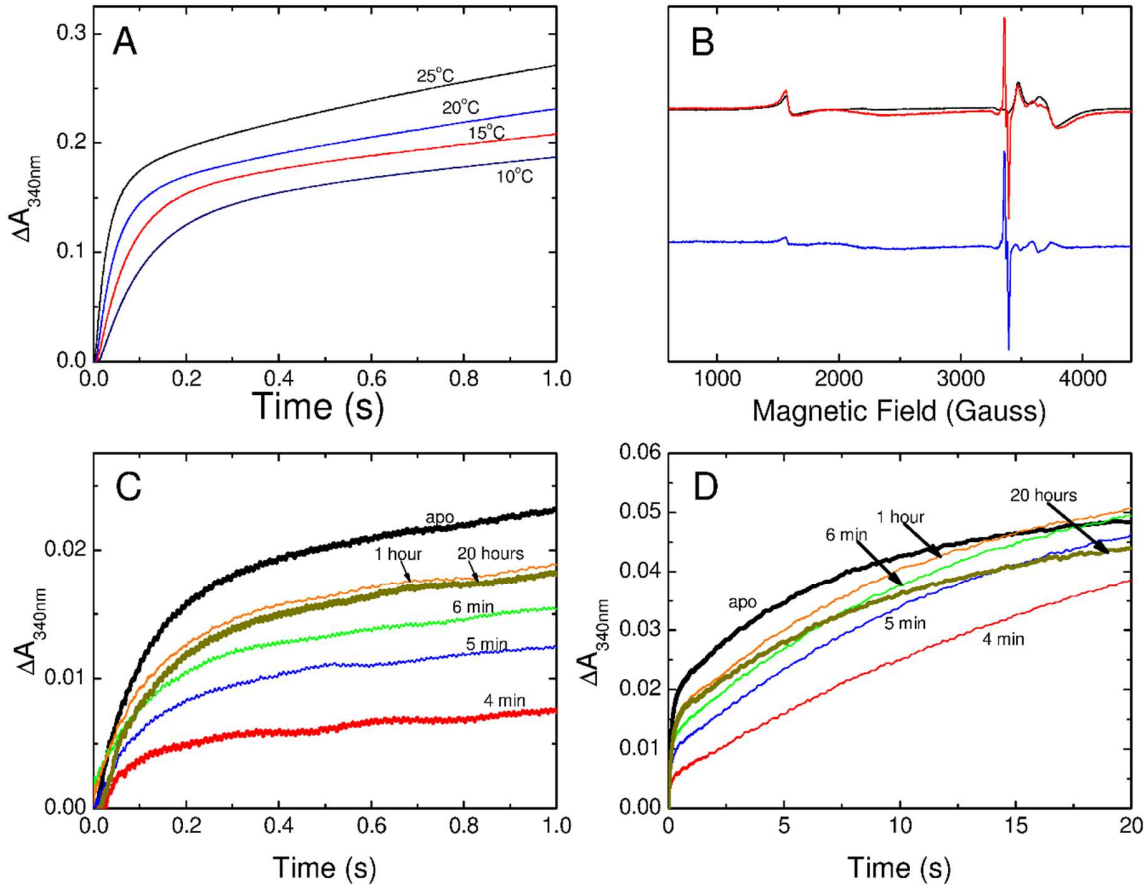

Figure S3. Properties of Fe^{2+} oxidation catalyzed by *Syn*Ftn. (**A**) The effect of temperature on the iron oxidation kinetics of *Syn*Ftn measured by stopped flow absorbance at 340 nm. A decrease in rate of the rapid oxidation phase was observed on lowering the temperature from 25 to 10 °C. Final protein concentration was 4.17 μM (100 μM in monomer) in each case, mixed with 72 molar equivalents of Fe^{2+}. (**B**) *Syn*Ftn continually generates the mixed valent form of the ferroxidase center during turnover. The EPR of *Syn*Ftn frozen 10 seconds after the addition of 72 Fe^{2+}/Ftn (red trace) and 20 seconds after the addition of 200 Fe^{2+}/Ftn (black trace). The blue trace is the difference between the spectra showing that the tyrosyl radical signal was eliminated under turnover conditions whilst the MVFC signal (at fields above 3400 G) was almost unaffected. Protein concentration was 4.17 μM in 24mer (100 μM *Syn*Ftn monomers) in each case. (**C**) and (**D**) Regeneration of rapid iron oxidation by *Syn*Ftn. (**C**) Absorbance at 340 nm as a function of time following mixing of apo *Syn*Ftn (black trace) or *Syn*Ftn incubated with 400 Fe^{2+}/Ftn for the times as indicated. Responses for apo protein and the longest incubation period are highlighted with a thicker trace. (**D**) Data as in (C) but showing the first 20 seconds of activity covering both rapid and slow phases of activity. Note that reversion of the slower phase of iron oxidation to that displayed by the apo protein is apparent only in the sample incubated for 20 hours.

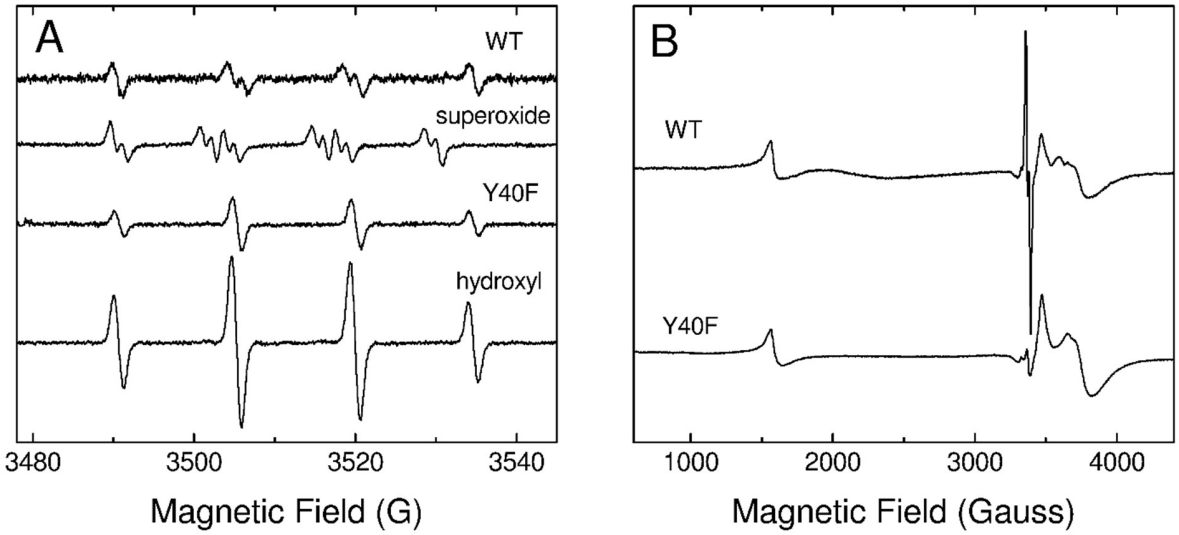

Figure S4. EPR analysis of Fe^{2+} oxidation catalyzed by *Syn*Ftn. (**A**) Superoxide is not the product of O_2 reduction by *Syn*Ftn. Room temperature EPR spectra recorded following the addition of 70 Fe^{2+}/Ftn to 5.35 μM wild type and Y40F *Syn*Ftn in 100 mM MES pH 6.5 in the presence of 40 mM DMPO. Reference spectra of the superoxide radical anion and hydroxyl radical adducts to DMPO were acquired as described in *Materials and Methods* and are shown for comparison. The small signal in the wild type *Syn*Ftn spectrum arises from a sulfite radical DMPO adduct (2) originating from an impurity in the MES buffer. (**B**) Y40F *Syn*Ftn does not give rise to a Tyr radical. Full field sweep EPR spectra of wild type and Y40F *Syn*Ftn in 100 mM MES pH 6.5 following the addition of 72 Fe^{2+}/*Syn*Ftn and freezing of the samples within 12 seconds. The feature at 1600 Gauss (g = 4.3) is indicative of mononuclear high spin Fe^{3+}. The sharp feature at approximately 3400 Gauss (g = 2) in the wild type spectrum is due to a tyrosyl radical and is absent in the Y40F variant, being replaced by a small EPR signal consistent with trace amounts of peroxyl radical.

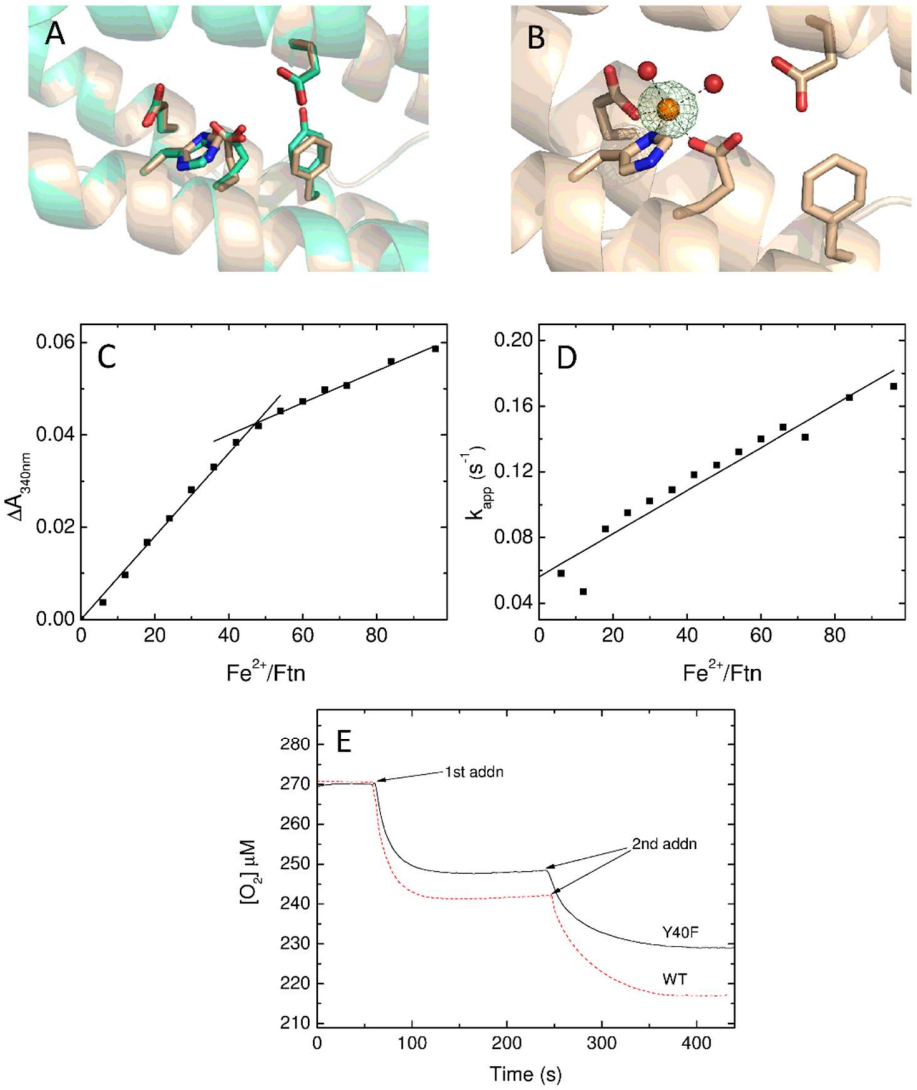

Figure S5. The Y40F variant of *Syn*Ftn. (**A**) The ferroxidase center of apo Y40F *Syn*Ftn at pH 6.5 (wheat) overlaid with the corresponding model for the wild type protein (cyan). (**B**) The ferroxidase center of Y40F *Syn*Ftn soaked in an aerobic Fe^{2+} solution at pH 6.5 for 2 minutes together with the anomalous difference map contoured at 8σ. (**C**) and (**D**) Analysis of iron oxidation by Y40F *Syn*Ftn monitored by stopped flow absorbance. (**C**) Amplitude of the absorbance change at 340 nm as a function of Fe^{2+} added per *Syn*Ftn. Trend lines represent linear fits to the data. (**D**) Apparent rate constant extracted for the oxidation of iron as a function of Fe^{2+} added per *Syn*Ftn. Protein (1.0 μM in 100 mM MES pH 6.5) was mixed with equal volumes of Fe^{2+} at the appropriate concentration and stabilized in 1 mM aqueous HCl. (**E**) O_2 consumption during Fe^{2+} oxidation by Y40F *Syn*Ftn. Change in dissolved O_2 concentration following successive additions of 48 equivalents (48 μM) of Fe^{2+} to 1 μM apo Y40F *Syn*Ftn at 20 °C (black trace). Data from an equivalent measurement on wild type *Syn*Ftn is shown for comparison (broken red trace). Lower O_2 consumption by Y40F is indicative of a higher Fe:O_2 reaction stoichiometry. We note that the lack of iron at site Fe_B following the iron soak is most likely a consequence of the slower

rate of Fe^{2+} oxidation in this variant compared to wild type protein. The affinity of site Fe_B for Fe^{2+} (in both wild type and Y40F) may not be very high due to the lack of coordinating ligands and so reaction with O_2, resulting in oxidation to the MVFC (that features a stabilizing hydroxo bridge), might be required to observe significant occupancy of this site.

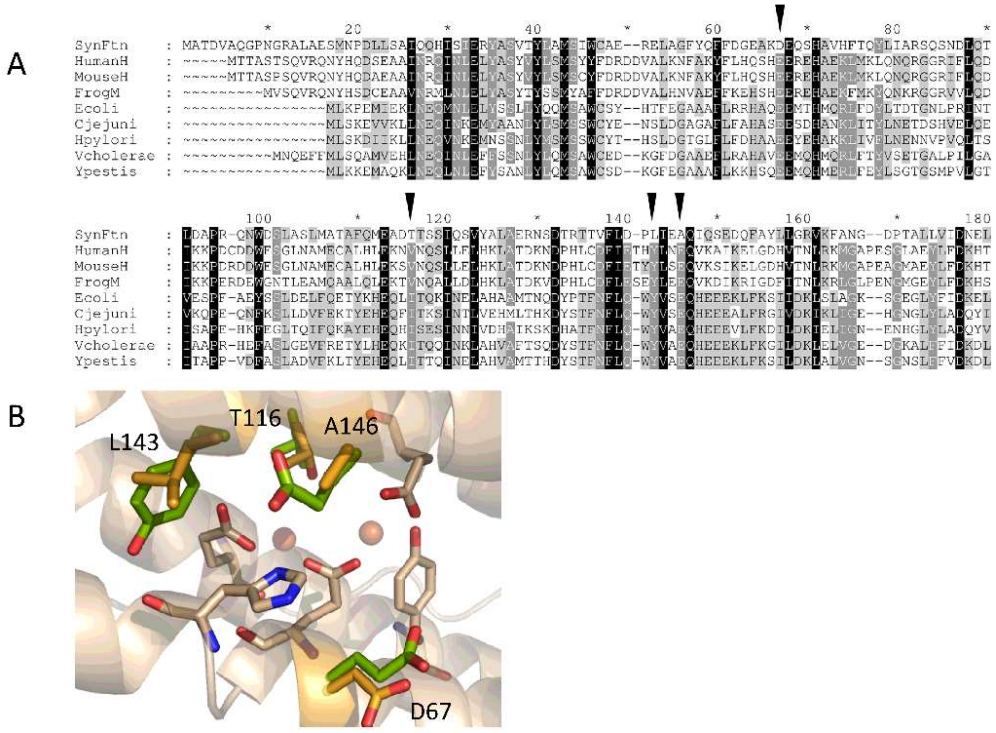

Figure S6. Conservation of near ferroxidase center residues in ferritins. (**A**) Sequence alignments of selected ferritins. Residues close to the catalytic center that are conserved in all sequences other than *Syn*Ftn are highlighted with black arrows. (**B**) The structure of *Syn*Ftn following aerobic soaking in a 5 mM Fe^{2+} solution for 2 min. Sidechains of the residues highlighted in (A) are shown in orange. Note that labelling of sidechains in panel (B) corresponds to the numbering in panel (A), including breaks in the sequence introduced for the purposes of alignment. For comparison, the equivalent sidechains from an aerobic Fe^{2+} soak of human H-chain ferritin (HuHF) are shown in green. Image produced using pdb entries 6GKC (*Syn*Ftn) and 4YKH (HuHF)((19)). Aligned protein sequences are human H-chain ferritin (HumanH), mouse H-chain ferritin (mouseH), frog M-chain ferritin (FrogM), *E. coli* FtnA (Ecoli), *Campylobacter jejuni* Ftn (Cjejuni), *Helicobacter pylori* Ftn (Hpylori), *Vibrio cholerae* Ftn (Vcholerae), and *Yesinia pestis* Ftn (Ypestis).

Table S1. X-ray diffraction data collection and refinement statistics for apo and iron-soaked wild type and Y40F *Syn*Ftn crystals.

	*Syn*Ftn apo	*Syn*Ftn 2 min Fe^{2+} soak	*Syn*Ftn 20 min Fe^{2+} soak
PDB Entry	5OUW	6GKC	6GKA
Data collection[a]			
Wavelength, Å	0.9795	0.9795	0.9795
Space group	F432	F432	F432
Cell parameter, Å	177.7	177.2	177.3
Resolution limits, Å	53.59 – 2.05 (2.10 – 2.05)	53.41 – 1.97 (2.02 – 1.97)	53.45 – 1.76 (1.80 – 1.76)
Unique reflections	15595(1110)	16769(1161)	23392 (1299)
Rmerge	0.074(0.640)	0.071(1.073)	0.052(0.731)
Rmeas	0.075(0.649)	0.084(1.283)	0.059(0.854)
Rpim	0.010(0.085)	0.044(0.685)	0.028(0.428)
$\langle I/\sigma(I)\rangle$	53.2(9.6)	12.3(1.1)	15.6(1.6)
CC(1/2)	1.00(0.986)	0.998(0.509)	0.999(0.585)
Completeness, %	99.7 (99.9)	100.0 (99.8)	97.1 (95.5)
Multiplicity	54.9(57.9)	3.3(3.2)	4.1(3.5)
Wilson B factor, $Å^2$	23.2	23.5	20.2
Refinement Statistics			
Protein monomers per ASU	1	1	1
Total atoms (non-hydrogen)	1556	1537	1636
Metal ions	0	2	3
Water molecules	148	135	222
Reflections used in refinement	15575(1513)	16762(1636)	23388(2273)
Reflections used for Rfree	706(76)	823(73)	1156(103)
Rwork, %	15.4(19.5)	17.7(26.9)	15.7(27.9)
Rfree, %	19.7(25.94)	20.1(31.2)	18.6(32.1)
Ramachandran Analysis, %			
Favoured	99.4	99.4	99.4
Outliers	0.0	0.0	0.0
Rotamer outliers, %	2.0	0.7	1.3
RMS deviations			
Bonds, Å	0.006	0.006	0.006
Angles, °	0.69	1.03	1.01
Planes, Å	0.004	0.004	0.004
Mean Atomic B-value, $Å^2$	31.9	32.6	28.6

	Y40F *Syn*Ftn apo	Y40F *Syn*Ftn 2 min Fe^{2+} soak
PDB Entry	5OUZ	6GKB
Data collection[a]		
Wavelength, Å	0.9795	0.9795
Space group	F432	F432
Cell parameter, Å	176.9	176.7
Resolution limits, Å	53.34 – 2.08 (2.14 – 2.08)	62.47 – 1.90 (1.94 – 1.90)
Unique reflections	14805(1069)	18124(1149)
Rmerge	0.076(0.658)	0.052(0.953)
Rpim	0.077(0.664)	0.059(1.091)
Rmeas	0.010(0.088)	0.028(0.516)
$\langle I/\sigma(I)\rangle$	46.9(8.5)	14.4(1.4)
CC(1/2)	1.000(0.985)	0.998(0.527)
Completeness, %	100 (100)	95.9(98.1)
Multiplicity	56.6(56.3)	4.1(4.0)
Wilson B factor, $Å^2$	29.4	27.6
Refinement Statistics		
Protein monomers per ASU	1	1
Total atoms	1532	1556
Metal ions	0	2
Water molecules	139	153
Reflections used in refinement	14800(1443)	18122(1793)
Reflections used for Rfree	752(63)	906(91)
Rwork, %	15.4(14.0)	16.7(25.7)
Rfree, %	20.4(26.1)	21.0(31.5)
Ramachandran Analysis, %		
Favoured	100	99.4
Outliers	0.0	0.0
Rotamer outliers, %	0.7	2.0
RMS deviations		
Bonds, Å	0.005	0.006
Angles, °	0.66	1.02
Planes, Å	0.004	0.003
Mean Atomic B-value, $Å^2$	37.3	39.5

[a] Statistics for the highest-resolution shell are shown in parentheses.

Table S2. Optimized anomalous scattering X-ray diffraction data collection statistics for iron soaked wild type and Y40F *Syn*Ftn crystals.

Data collection[a]	*Syn*Ftn 2 min Fe^{2+} soak	*Syn*Ftn 20 min Fe^{2+} soak	Y40F *Syn*Ftn 2 min Fe^{2+} soak
Wavelength, Å	1.7399	1.7389	1.7399
Space group	F432	F432	F432
Cell parameter, Å	177.2	177.0	176.8
Resolution limits, Å	102.3-2.50 (2.60-2.50)	102.2-2.50 (2.60-2.50)	102.1-2.50 (2.60-2.50)
Number unique reflections	8748(955)	8702(944)	8684(961)
Rmerge	0.114(0.550)	0.063(0.256)	0.057(0.238)
Rmeas	0.116(0.557)	0.066(0.268)	0.058(0.241)
Rpim	0.018(0.089)	0.020(0.081)	0.009(0.038)
$\langle I/\sigma(I)\rangle$	45.2(13.0)	35.4(10.9)	77.1(25.0)
CC(1/2)	0.999(0.993)	0.999(0.991)	1.000(0.998)
Δanom CC(1/2)	0.773(0.219)	0.701(0.156)	0.773(0.313)
Anomalous completeness, %	100(100)	100(100)	100(100)
Anomalous multiplicity	40.3(38.9)	11.2(10.6)	41.1(39.3)
Wilson B factor, $Å^2$	23.4	30.4	32.6

[a] Statistics for the highest-resolution shell are shown in parentheses.

Table S3. Metal binding site statistics.

Sample	Site[1]	Metal	Ligands	Occupancy[2]	B factor (Metal)[3]	B factor (Env.)[3]	Geometry
WT 2 min Fe^{2+} soak	1	Fe	O_4N_1	0.50	41.8	41.9	Trigonal Bipyramidal
	2	Fe	O_5	0.56	48.2	48.2	Octahedral
WT 20 min Fe^{2+} soak	1	Fe	O_4N_1	0.90	27.5	29.8	Octahedral
	2	Fe	O_6	0.55	31.8	35.0	Octahedral
	3	Fe	O_6	0.28	27.9	29.0	Octahedral
Y40F 2 min Fe^{2+} soak	1	Fe	O_4N_1	0.75	41.8	45.5	Trigonal Bipyramidal
	3	Fe	O_3	0.2	62.6	63.8	Tetrahedral

[1] Site 1 refers to Fe_A and site 2 to Fe_B.
[2] Site 3 is in a three-fold channel and sits on the 3-fold axis. It has a maximal occupancy of 0.33.
[3] The equivalent isotropic temperature factor (units $Å^2$) for the metal ion ('Metal') is shown alongside the average for atoms in its coordination environment ('Env.')

Table S4. The simulation parameters for the Tyr radical EPR spectrum of *Syn*Ftn during iron oxidation (Fig. 5A) as determined by TRSSA with an input of θ = -4° and ρ_{C1} = 0.395. The *inset* shows the neutral tyrosyl radical structure with atom nomenclature.

g_x	g_y	g_z
2.00743	2.00427	2.00220

ΔH_x, Gauss	ΔH_y, Gauss	ΔH_z, Gauss
6.23	4.66	4.52

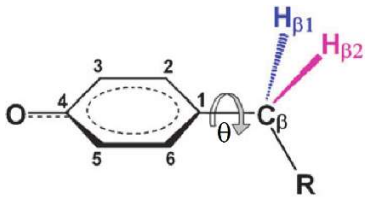

Protons hyperfine coupling matrix principal values[a]			**Euler angle**[b] Φ_1	**Euler angle** Φ_2	**Euler angle** Φ_3
$A^{\beta1}_{cc}$, MHz	$A^{\beta1}_{bb}$, MHz	$A^{\beta1}_{aa}$, MHz	$-\Phi_1^{\beta1}$, degree	$-\Phi_2^{\beta1}$, degree	$-\Phi_3^{\beta1}$, degree
63.06	56.35	56.35	-10.2	-34.8	-82.6
$A^{\beta2}_{cc}$, MHz	$A^{\beta2}_{bb}$, MHz	$A^{\beta2}_{aa}$, MHz	$-\Phi_1^{\beta2}$, degree	$-\Phi_2^{\beta2}$, degree	$-\Phi_3^{\beta1}$, degree
18.89	15.35	15.35	29.5	4.1	50.4
A^{C3}_{cc}, MHz	A^{C3}_{bb}, MHz	A^{C3}_{aa}, MHz	$-\Phi_1^{C3}$, degree	$-\Phi_2^{C3}$, degree	$-\Phi_3^{C3}$, degree
-25.9	-8.1	-20.5	23.0	0.0	0.0
A^{C5}_{cc}, MHz	A^{C5}_{bb}, MHz	A^{C5}_{aa}, MHz	$-\Phi_1^{C5}$, degree	$-\Phi_2^{C5}$, degree	$-\Phi_3^{C5}$, degree
-25.9	-8.1	-20.5	-23.0	0.0	0.0
A^{C2}_{cc}, MHz	A^{C2}_{bb}, MHz	A^{C2}_{aa}, MHz	$-\Phi_1^{C2}$, degree	$-\Phi_2^{C2}$, degree	$-\Phi_3^{C2}$, degree
7.5	5.0	1.5	40.0	0.0	0.0
A^{C6}_{cc}, MHz	A^{C6}_{bb}, MHz	A^{C6}_{aa}, MHz	$-\Phi_1^{C6}$, degree	$-\Phi_2^{C6}$, degree	$-\Phi_3^{C6}$, degree
7.5	5.0	1.5	-40.0	0.0	0.0

[a] The three principal components of A tensors are A_{aa}, A_{bb} and A_{cc}.

[b] Three Euler angles are the three rotations of tensor A, Φ_1 - around Z-axis , Φ_2 - around Y and Φ_3 - around X, required to bring aa direction of A with X, bb with Y and cc with Z axes.

Table S5. Ring rotation angle θ in the six tyrosines of a monomer of *Syn*Ftn (PDB code 6GKC). While the simulated free radical EPR spectrum was optimized for the ring rotation angle of -4° (Fig. 5A), another, geometrically complementary angle of -56° would yield an identical set of values of the electron spin hyperfine interaction with the two methylene protons spins. Therefore, the Tyr residues in the protein structure were analysed for their proximity to both values of the ring angle obtained from the simulation. (A) Sorted by proximity to the value of -4°. (B) Sorted by proximity to the value of -56°. The table shows that only Tyr40 has the ring in the rotational conformation close to the value of -4°, found from the simulation, and none has the conformation close to -56 °.

A			**B**		
Tyrosine	**θ °**	**|θ–(–4)|°**	**Tyrosine**	**θ °**	**|θ–(–56)|°**
A Tyr40	**-0.47**	**3.5**	A Tyr40	-0.47	55.5
A Tyr121	52.91	56.9	A Tyr121	52.91	108.9
A Tyr152	67.44	71.4	A Tyr152	67.44	123.4
A Tyr56	74.48	78.5	A Tyr56	74.48	130.5
A Tyr35	74.84	78.8	A Tyr35	74.84	130.8
A Tyr76	85.16	89.2	A Tyr76	85.16	141.2

Dataset S1. Cyanobacteria that contain a *Syn*Ftn homologue, a standard prokaryotic ferritin (containing a site C) or neither. Please see the associated file Dataset S1.xlsx.

Supporting References

1. Marchetti A, et al (2009) Ferritin is used for iron storage in bloom-forming marine pennate diatoms. *Nature* 457:467-470.
2. Ranguelova K, et al (2010) Protein radical formation resulting from eosinophil peroxidase-catalyzed oxidation of sulfite. *J Biol Chem* 285:24195-24205.